Behavioral/Cognitive

Alpha Oscillations Modulate Preparatory Activity in Marmoset Area 8Ad

Kevin Johnston,[1] Liya Ma,[1] Lauren Schaeffer,[2] and Stefan Everling[1,2]

[1]Department of Physiology and Pharmacology, The University of Western Ontario, London, Ontario N6A 3K7, Canada, and [2]Robarts Research Institute, The University of Western Ontario, London, Ontario N6A 5B7, Canada

Cognitive control often requires suppression of prepotent stimulus-driven responses in favor of less potent alternatives. Suppression of prepotent saccades has been shown to require proactive inhibition in the frontoparietal saccade network. Electrophysiological evidence in macaque monkeys has revealed neural correlates of such inhibition in this network; however, the interlaminar instantiation of inhibitory processes remains poorly understood because these areas lie deep within sulci in macaques, rendering them inaccessible to laminar recordings. Here, we addressed this gap by exploiting the mostly lissencephalic cortex of the common marmoset (*Callithrix jacchus*). We inserted linear electrode arrays into areas 8Ad—the putative marmoset frontal eye field—and the lateral intraparietal area of two male marmosets and recorded neural activity during performance of a task comprised of alternating blocks of trials requiring a saccade either toward a large, high-luminance stimulus or the inhibition of this prepotent response in favor of a saccade toward a small, low-luminance stimulus. We observed prominent task-dependent activity in both alpha/gamma bands of the LFP and discharge rates of single neurons in area 8Ad during a prestimulus task epoch in which the animals had been instructed which of these two tasks to perform but before peripheral stimulus onset. These data are consistent with a model in which rhythmic alpha-band activity in deeper layers inhibits spiking in upper layers to support proactive inhibitory saccade control.

Key words: eye movement; frontal cortex; marmoset; parietal cortex; saccade

Significance Statement

Failures to inhibit automatic saccadic responses are a hallmark of many neuropsychiatric disorders, but how this process is implemented across the cortical layers in the frontoparietal saccade network remains unknown because many of the areas are inaccessible to laminar recordings in macaques. Here, we investigated laminar neural activity in marmoset monkeys, which have a smooth cortex. Monkeys were required either to generate or inhibit a prepotent saccade response. In area 8Ad, the putative frontal eye field in marmosets, rhythmic alpha-band activity (9–14 Hz) was higher in deeper layers and spiking activity was lower in upper layers when the animals were instructed to suppress a saccade toward a peripheral stimulus. Reduced alpha power during task preparation may be the underlying common neural basis of a saccade suppression deficit.

Introduction

A fundamental aspect of executive control is the ability to respond flexibly to events in the environment (Miller and Cohen, 2001). Flexible responding often requires overriding prepotent stimulus-driven responses in favor of less potent alternatives. A popular saccadic eye movement paradigm that probes this ability is the antisaccade task (Munoz and Everling, 2004; Antoniades et al., 2013), which requires participants to suppress a saccade toward a suddenly appearing peripheral stimulus in favor of a saccade away from that stimulus. Performance in this task is typically contrasted with a simple prosaccade task requiring a saccade toward the stimulus. Although patients with a variety of neuropsychiatric disorders show normal saccade behavior in the prosaccade task (Everling and Fischer, 1998; Hutton and Ettinger, 2006), they often exhibit difficulty in suppressing saccades toward the stimulus in the antisaccade task, a finding consistent with an impairment of executive control.

Functional imaging studies have shown that a network of frontoparietal areas is more active for antisaccades than for prosaccades (O'Driscoll et al., 1995; DeSouza et al., 2003) and that many areas are already more active during preparatory periods

Received Oct. 18, 2018; revised Jan. 3, 2019; accepted Jan. 4, 2019.

Author contributions: K.J., L.M., L.S., and S.E. edited the paper; S.E. wrote the first draft of the paper. K.J. and S.E. designed research; K.J., L.S., and S.E. performed research; L.M. and S.E. analyzed data.

This work was supported by the Canadian Institutes of Health Research (Grant FRN148365 to S.E.) and the Canada First Research Excellence Fund to BrainsCAN. We thank Nicole Hague and Katherine Faubert for excellent animal care and surgical support.

The authors declare no competing financial interests.

Correspondence should be addressed to Stefan Everling at severlin@uwo.ca.

https://doi.org/10.1523/JNEUROSCI.2703-18.2019

Copyright © 2019 the authors 0270-6474/19/391855-12$15.00/0

when subjects look at an initial fixation stimulus before the peripheral stimulus appears (Connolly et al., 2002; Curtis and D'Esposito, 2003; DeSouza et al., 2003; Brown et al., 2007). In the macaque frontal eye fields (FEFs), saccade-related neurons are less active during the preparatory period on antisaccade than prosaccade trials and more active on erroneous antisaccade trials in which the monkey fails to suppress a saccade toward the stimulus (Everling and Munoz, 2000). These findings indicate that correct antisaccade performance requires proactive inhibition of saccade neurons in FEFs, which in turn decreases excitatory drive to the superior colliculus (SC), leading to reduced saccade preparation on antisaccade trials (Munoz and Everling, 2004).

Such proactive inhibition of saccade-related activity might be mediated by alpha-band oscillations because magnetocephalography (MEG) recording studies in human participants have reported increased alpha power on antisaccade trials and reduced alpha power on error trials in the FEFs (Hwang et al., 2014). However, the neural mechanisms by which alpha power may inhibit activity of FEF neurons remain to be determined.

Recently, it has been demonstrated that alpha power in deep cortical layers of macaque frontal cortex suppress gamma power and spiking activity in upper cortical layers (Bastos et al., 2018). Such a mechanism has previously been shown in visual cortex, where slower oscillations are prominent in deep layers (Maier et al., 2010; Buffalo et al., 2011; van Kerkoerle et al., 2014) and where the phase of deep alpha modulates the amplitude of upper gamma (Spaak et al., 2012). Accordingly, deep alpha in the FEFs might suppress gamma and spiking activity in upper FEF layers when prepotent saccade responses must be suppressed. Unfortunately, evaluating this model in macaque monkeys is practically intractable because the FEFs lie in the anterior bank of the arcuate sulcus (Bruce and Goldberg, 1985; Bruce et al., 1985), making this area inaccessible to laminar-specific recordings.

To address this, we adopted the common marmoset (*Callithrix jacchus*) model because these New World primates have a lissencephalic (smooth) cortex amenable to laminar recordings. For this species, we used a simplified version of the antisaccade task that retained the response suppression and voluntary saccade generation components but did not require a vector inversion of the stimulus location into a saccade command. We simultaneously recorded LFPs and single neuron activity with laminar electrodes in frontal area 8Ad, the putative homolog of FEFs in marmosets (Ghahremani et al., 2017), and in the lateral intraparietal (LIP) cortex during performance of this task. We observed prominent task-dependent activity in alpha/gamma bands and single neuron activity during the preparatory period, which is consistent with the hypothesis that deeper alpha inhibits spiking activity in upper layers for proactive saccade control in the FEFs.

Materials and Methods

Subjects. Two male marmoset monkeys (*Callithrix jacchus),* Marmoset M and Marmoset B, aged 5 and 4 years, respectively, and weighing ~360 g, were the subjects in this study. All experimental methods described were performed in accordance with the guidelines of the Canadian Council on Animal Care policy on the care and use of experimental animals and an ethics protocol approved by the Animal Care Committee of the University of Western Ontario. Monkeys were kept under the close supervision of the university veterinarians. Using previously described surgical, training, and experimental techniques (Johnston et al., 2018), both monkeys were implanted with a custom-built oval-shaped recording chamber that incorporated four conical receptacles that were used to fixate the chamber in a custom-built stereotaxic frame during the experimental sessions. After training on the behavioral paradigm, burr holes (~3 mm in diameter) were drilled within the chamber in a second surgery to allow access to area 8Ad (15 mm anterior, 4 mm lateral) and area LIP (1.5 mm anterior 6 mm lateral).

Behavioral task. We initially attempted to train marmosets on a prosaccade/antisaccade task comparable to what we have regularly used in macaque monkeys (Munoz and Everling, 2004). During training, however, it became apparent that some aspects of this task were exceptionally difficult for marmosets, as evidenced by their poor task performance. One aspect was task mixing. We have often presented prosaccade and antisaccade trials interleaved in random order, with the shape or color of the central fixation point serving as a task instruction. Marmosets performed poorly on this version of the task, so we instead resorted to task blocks of prosaccade and antisaccade trials, as is the case in most studies using human participants (Antoniades et al., 2013). The other aspect was difficulty in generating saccades to an empty visual hemifield. Both marmosets made many errors when required to perform an antisaccade to a blank location on the display monitor. We therefore used the final stage of the antisaccade training protocol for macaque monkeys, in which a dim, very small stimulus cues the target location on antisaccade trials (Johnston and Everling, 2011). This task retains the cognitive components of response inhibition and voluntary saccade generation central to the antisaccade task, but does not require the vector inversion process necessary for generation of saccades to an empty location.

Animals were required to first fixate a central instruction cue presented at the center of a dark CRT display (0.01 cd/m^2) within an electronic window of 4° × 4° surrounding it for a duration of 500–700 ms. For Marmoset M, a cross (1° × 1°, 10 cd/m^2) signaled a prosaccade trial and a filled circle (0.55°, 10 cd/m^2) signaled an antisaccade trial. The instructions were reversed for Marmoset B. Following this, two circular stimuli were presented simultaneously to the left and right equidistant from fixation at an eccentricity of 6.7°. One of the stimuli was larger (1.6°) and of higher luminance (20 cd/m^2) than the other (.2°, 1.5 cd/m^2). Animals were required to generate a single saccade toward either the more (prosaccade trials) or less (antisaccade trials) salient stimulus, depending on the shape of the central instruction cue to obtain a liquid reward (diluted sweetened condensed milk for Marmoset B and diluted corn syrup for Marmoset M; monkeys were not on any liquid control schedule). After 10 correctly performed trials, the task reversed. Monkeys would perform this task reliably for durations varying between 25 and 45 min. The experimental paradigm was presented under the control of the CORTEX real-time operating system (National Institutes of Mental Health–National Institutes of Health, Bethesda, MD) running on two Pentium PCs. The program also monitored the animals' behavior and controlled reward delivery.

Recording technique. Monkeys were seated in a primate chair that integrated with a custom designed stereotaxic frame for head restraint and mounting of microelectrode drives. The chair/frame system was mounted on a table within a sound-attenuating chamber (Crist Instrument). Their heads were restrained and a liquid spout placed at their mouths for computer-controlled reward delivery (Crist Instrument). Eye positions were monitored via high-speed (1000 Hz) monocular video tracking of the pupil (EyeLink 1000, SR Research).

Extracellular laminar recordings were made from area 8Ad and area LIP with commercially available silicon-based 16 contact microelectrodes with 150 μm interelectrode spacing (ATLAS Neuroengineering) that were inserted into the cortex vertical to the interaural plane with electrode micromanipulators (Kopf Instruments) attached to the stereotaxic frame at the beginning of each recording session. To ensure a relatively unbiased sampling of neural activity, we did not prescreen neurons for task-related responses. Instead, we slowly advanced one laminar electrode into area 8Ad and one into area LIP until most of the contacts were inside the brain, as determined by monitoring LFPs at each electrode contact. We waited ~20 min to allow the electrodes to settle before commencing behavioral and neural data collection.

Neural activity (LFPs and spiking activity) was amplified, filtered, and stored for offline data analysis using the Plexon MAP system for one monkey and the Open Ephys acquisition board (http://www.open-ephys.org) and digital head stages (INTAN) in the other. Data collected with both systems were offline converted to Neuroexplorer (nex) files

and single units were isolated by applying principal component analysis in 2D and 3D with the Plexon offline sorter. Horizontal and vertical eye positions and the occurrence of behavioral events (e.g., start of trial, onset of fixation, stimulus presentation, reward delivery, performance) were also stored.

Data analysis. Analysis was performed with custom MATLAB code (The MathWorks) and the fieldtrip toolbox (http://www.ru.nl/fcdonders/fieldtrip/). We limited all analyses to the preparatory period from 500 ms to 0 s before peripheral stimulus onset, excluding stimulus- and saccade-related activity occurring later in the trial. We included only single neurons with at least 10 trials in each task condition (e.g., ≥10 correct prosaccades and ≥10 correct antisaccades).

Oscillatory LFP activity was calculated for the different electrode contacts in selected frequency bands (alpha: 9–14 Hz, gamma: 60–150 Hz) based on Hanning tapered Fourier transforms for the 500 ms preparatory window after removal of the powerline artifacts at 60 and 120 Hz using a discrete Hamming band-stop filter. Data were analyzed across recording sessions by aligning electrode contacts to the cortical surface, which was easily identified by a prominent increase in LFP power (see Fig. 1*D*).

The effects of electrode depth and task on alpha and gamma power were analyzed with repeated-measures ANOVAs with the factors depth at 9 levels (150, 300, 450, 600, 750, 900, 1050, 1200, and 1350 μm below the cortical surface) and task at 2 levels (correct prosaccades and correct antisaccades). The effects of electrode depth and performance on alpha and gamma power were analyzed with repeated-measures ANOVAs with the factors depth at 9 levels (150, 300, 450, 600, 750, 900, 1050, 1200, and 1350 μm below the cortical surface) and performance at 2 levels (erroneous antisaccades and correct antisaccades).

To test whether alpha or gamma power in area 8Ad could predict performance on antisaccade trials on a trial-by-trial basis, we performed linear discriminant analyses. We randomly selected the same number of correct antisaccade and error trials from each session (i.e., 20 correct antisaccade trials and 20 error trials from a file that had 50 correct antisaccade trials and 20 error trials). We then used half of the correct and half of the error antisaccade trials to train a linear discriminant analysis model with the alpha or gamma power recorded at each electrode contact using MATLAB's *fitcdiscr* function and the other half of the trials to test the model's prediction using the *predict* function. These steps were repeated 200 times to obtain distributions of prediction rates (between 0% and 100%) for each recording session, which we then tested against the chance median of 50 using Wilcoxon signed-rank tests evaluated at $p < 0.001$.

To identify the effect of alpha troughs in deep layers on single neuron activity, we filtered the LFP recorded at 1350 μm below the cortical surface for all trials on which the monkeys maintained central fixation until the peripheral stimulus was presented. This was accomplished using a Hamming band-pass filter between 9 and 14 Hz, followed by the identification of the troughs of the alpha cycles in the 500 ms period before stimulus presentation using MATLAB's *findpeaks* function on the inverted filtered LFP. We then aligned single neuron activity, convolved with a 15 ms Gaussian filter, on the troughs of the alpha cycles. Neural activity was compared between activity around the peak (−50 to −30 ms before the trough) and the trough of the alpha cycle (−10 to 10 ms). A modulation index was computed to compare the effects of the strength of the alpha trough on neural activity through the following formula: (peak_activity − trough activity)/(peak_activity + trough activity).

To characterize the cross-frequency correlations in the LFPs, especially those between the alpha and gamma bands, we calculated Tort's modulation index (MI) using the methods detailed previously (Voloh et al., 2015; Tort et al., 2010). Variable band-pass filters defined as ±1/3 of the center frequency were used to filter the raw LFP signals, which were then Hilbert transformed (Voloh et al., 2015). We calculated the MI between the phases of low-frequency bands centered between 4.5 and 30 Hz (with 1.5 Hz steps) and the amplitudes of high-frequency bands centered between 30 and 159 Hz (with 3 Hz steps). The phases and amplitudes used in each calculation of MI were always from different channels to avoid spurious coupling within channel (Tort et al., 2010). For a given channel pair, we binned ($n = 18$ bins) the phases extracted from the phase-providing channel; the amplitudes from the amplitude-providing channel were then binned according to the phases and averaged within each bin. Finally, the amplitude from each bin was normalized by the mean of amplitudes from all bins. The Kullback–Leibler (KL) distance, which is used to quantify the difference between the distribution of amplitudes across the phase bins and a uniform distribution, is calculated as follows:

$$D(P,Q) = \sum_{j=1}^{N} P(j) \cdot \log\left(\frac{P(j)}{Q(j)}\right)$$

Where P is the observed distribution, Q is the uniform distribution with the same mean amplitudes, j is an individual phase bin, and N is the total number of phase bins. The MI is then calculated as the normalized KL distance as follows:

$$MI = \frac{D(P,Q)}{\log(N)}$$

The MI equals to the normalized Shannon entropy of the gamma amplitude distribution across the low-frequency oscillation phase bins minus 1, the entropy of the uniform distribution.

To determine the significance of the MI values, we also calculated surrogate MI values by randomly dividing the high-frequency amplitude signal in two and reconnecting them in reversed order while keeping the low-frequency phase signal the same (Voloh et al., 2015). This way, the temporal structures within the phase and the amplitude signals were mostly maintained, but any potential correlation between the two was disrupted. This procedure was repeated 200 times (Voloh et al., 2015). To identify the cross-frequency correlation specifically associated with the antisaccade rule, we calculated the rule selectivity index (RSI) as follows:

$$RSI = \frac{MI_{Anti} - MI_{Pro}}{MI_{Anti} + MI_{Pro}}$$

The RSIs were also calculated for the surrogate data. Following a method described previously (Maris and Oostenveld, 2007), we then performed a cluster-based permutation test based on paired t statistic between the RSIs from real and those from surrogate data to determine the significant cross-frequency correlations during antisaccade trials (see Fig. 5*C*). Specifically, a map of t statistics was calculated between real and surrogate data. The significance level was then determined from a distribution of t statistics generated by 1000 iterations of pooling and random splitting of the data. Original t statistics that were >99.9% of the generated distribution were considered significant. Significant t statistics were then clustered using the *clusterdata* function in MATLAB.

The MI also allowed us to determine the preferred phase of alpha oscillation (9–14 Hz) of gamma activities. This was calculated as circular mean across the phase bins weighted by the amplitude and its probability. Each channel pair produced a single preferred phase bin. We then constructed the distributions of preferred phases of all channel pairs during the correct trials under the prosaccade and antisaccade rules and errors under the antisaccade rule (see Fig. 5*D*). The polarity of each distribution was determined using Rayleigh's test using the CircStat toolbox (Berens, 2009). The presence of difference between the preferred phase distributions from correct prosaccade and antisaccade trials and between correct and erroneous antisaccade trials was determined using the χ^2 goodness of fit test.

To determine whether the erroneous prosaccades made on antisaccade trials (referred to as the "errors" in short) were preceded by gamma activities with similar preferred alpha phases to those preceding correct antisaccades; we also compared two difference distributions: one between correct prosaccades and errors and the other between correct antisaccades and errors. To do this, we calculated the difference in the products of gamma amplitudes and their corresponding probability between correct trials (either prosaccade or antisaccade) and the errors. We then computed the circular mean across all bins and the corresponding preferred phases of these difference distributions. Again, each channel pair now produced a single preferred phase bin. Finally, we applied the χ^2 goodness of fit test to the two sets of count data (each channel pair

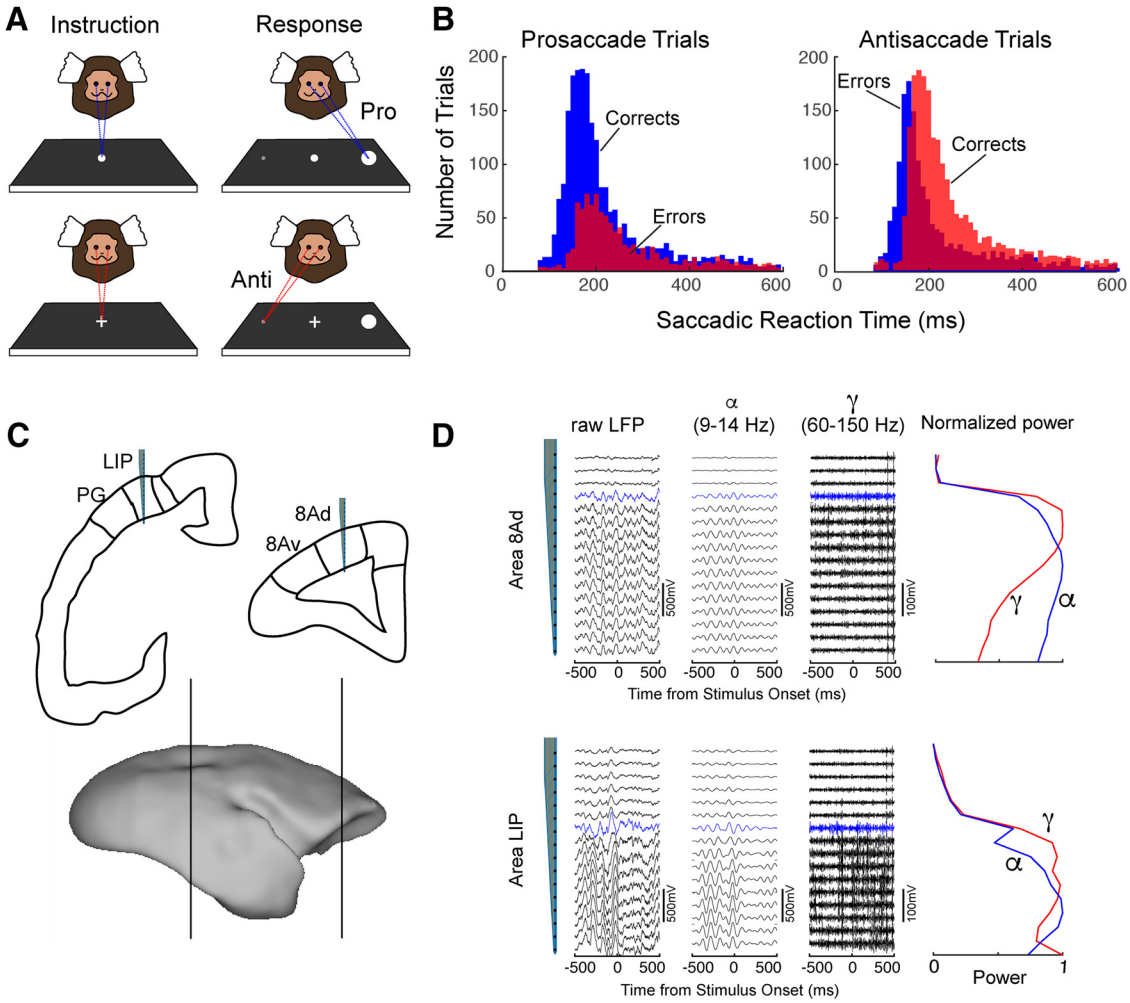

Figure 1. Task, behavior, and neural recordings. ***A***, Blocked prosaccade and antisaccade task adapted for marmosets. Animals were presented with a central instruction stimulus and required to generate a saccade toward a highly salient (top, prosaccade trials) or a small, dim stimulus (bottom, antisaccade trials) to receive a liquid reward. ***B***, Saccadic reaction times for correct (blue bars) and error (red bars) responses on prosaccade (left) and antisaccade (right) trials. ***C***, Recording locations. Top, Coronal sections of parietal and frontal cortex depicting locations of electrode penetrations with respect to cytoarchitecturally defined regions of marmoset cortex. Sections correspond to rostrocaudal locations marked on a lateral view of marmoset brain presented at the bottom. ***D***, Example recordings depicting raw LFP, alpha, gamma, and normalized alpha and gamma power across time as a function of electrode contact depth for area 8Ad (top) and Area LIP (bottom). Blue traces in LFP signals indicate depth of first contact identified as lying within cortex. This landmark was used as the basis for depth categorization in subsequent analyses.

contributed one count) across phase bins in the same way that we tested the original distributions.

Results

Behavior

We recorded laminar neural activity in 16 sessions in Marmoset M and 15 sessions in Marmoset B while they performed alternating blocks of prosaccade and antisaccade trials (Fig. 1*A*). Figure 1*B* shows the distribution of saccade reaction times (SRTs) for the saccades recorded in those sessions. Figure 1*B*, left, shows correct prosaccades (blue) and response errors (red); that is, saccades away from the large stimulus to the small stimulus. Figure 1*B*, right, shows the distribution of correct antisaccades (red) and erroneous saccades toward the large stimulus (blue). Prosaccades had significantly shorter SRTs than antisaccades (mean ± SD; 209 ± 100 ms vs 229 ± 98 ms, two-sample *t* test, $t_{(3973)} = 5.68$, $p = 1.4 \times 10^{-8}$). In addition, errors on prosaccade trials (255 ± 114 ms) had longer SRTs than correct prosaccades (two-sample *t* test, $t_{(2906)} = 10.46$, $p < 1 \times 10^{-14}$) and errors on antisaccade trials (201 ± 98 ms) had shorter SRTs than correct antisaccades (two-sample *t* test, $t_{(3327)} = 7.22$, $p = 6 \times 10^{-13}$). Monkeys also made more errors on the antisaccade trials (1371/3329 or 41%) than on prosaccade trials (891/2908 or 31%) ($\chi^2 = 74.66$, df = $p = 5.6 \times 10^{-18}$). Together, the longer SRTs and higher error rates on antisaccade trials indicate that the antisaccade task was more difficult for the marmosets than the prosaccade task, consistent with the behavior of macaques (Everling et al., 1999; Bell et al., 2000) and human subjects (Everling and Fischer, 1998).

Figure 1*C* shows a schematic of the recording locations in area LIP and 8Ad in the marmoset. These areas were identified based on the cytoarchitectonic atlas (Paxinos et al., 2012) and on the results of an fMRI functional connectivity study (Ghahremani et al., 2017). Example laminar activity in areas 8Ad and LIP on a single trial is illustrated in Figure 1*D*. LFP power clearly increased once electrode contacts entered the cortex (Fig. 1*D*, blue lines). In frontal cortex, gamma power was maximal in the upper layers and then decreased in deeper layers, whereas alpha power was higher in deeper than upper layers. We did not find any such differences between alpha and gamma power in parietal cortex.

In this study, we were interested in potential task-related differences in neural activity during the preparatory period before peripheral stimulus presentation during which the animal had been instructed to perform either a prosaccade or an antisaccade, but did not yet know in which hemifield the large and small stimuli would be presented. We therefore combined trials with left and rightward saccades and limited the analysis to the 500 ms period immediately before peripheral stimulus onset, during which the animals were required to maintain central fixation (Fig. 2*A*). We first looked at the LFP power during this period. Figure 2*B* shows an example power spectrum for electrode contacts 150 μm below the cortical surface (dashed lines) and 1200 μm below the surface (solid lines) in area 8Ad on antisaccade (red) and prosaccade (blue) trials. The spectrum shows a clear peak in alpha power (9–14 Hz) that was larger for antisaccade trials and stronger on the deeper electrode contact than the upper electrode contact. In contrast, we observed higher gamma power (60–150 Hz) at the upper than at the deeper electrode contacts. Moreover, gamma power was higher for prosaccades than for antisaccades.

We next quantified these single session differences across recording sessions. We included 23 sessions in which we recorded in area 8Ad and for which at least nine of the 16 electrode contacts were identified as within the cortex. Figure 2*C*, top left, shows the alpha power for prosaccade (blue) and antisaccade (red) trials across cortical depth. A two-way repeated-measures ANOVA showed a strong main effect of depth ($F_{(8,176)} = 40.0$, $p < 1 \times 10^{-11}$), a main effect of task ($F_{(1,22)} = 7.73$, $p = 0.011$), and a strong interaction effect of depth with task ($F_{(8,22)} = 7.87$, $p = 5 \times 10^{-9}$). For gamma power (60–150 Hz) depicted in Figure 2*C*, top right, we found a significant effect of depth ($F_{(8,176)} = 8.55$, $p = 8.3 \times 10^{-10}$) and task ($F_{(1,22)} = 5.48$, $p = 0.029$), but not for the interaction ($F_{(8,22)} = 1.07$, $p = 0.38$). These results show stronger alpha power for antisaccade trials at the deeper cortical depths and higher gamma power across cortical depth on prosaccade trials. This analysis demonstrates that alpha power in the deeper cortical layers is reduced and gamma power across cortical layers is increased on erroneous antisaccade trials.

The results were similar for the comparison of correct antisaccade trials (red) with error trials, shown in Figure 2*C*, bottom. A two-way ANOVA showed a significant main effect of depth ($F_{(8,176)} = 39.21$, $p < 1 \times 10^{-10}$), no main effect of performance ($F_{(1,22)} = 1.13$, $p = 0.30$) but a significant interaction between depth and performance ($F_{(8,22)} = 2.59$, $p = 0.01$) for alpha power. Gamma power showed a main effect of depth ($F_{(8,2176)} = 8.62$, $p < 6.9 \times 10^{-10}$) and performance ($F_{(1,22)} = 11.70$, $p < 0.0024$), but no interaction effect ($F_{(8,22)} = 1.25$, $p = 0.27$).

For the 27 sessions in area LIP with at least 9 electrode contacts in cortex, there was a significant effect for alpha power (Fig. 2*D*, top) in the factor depth ($F_{(8,208)} = 32.29$, $p < 1 \times 10^{-20}$), but not in task ($F_{(1,26)} = 2.27$, $p = 0.14$), and no interaction between depth and task ($F_{(8,26)} = 1.19$, $p = 0.31$). This was similar when we compared alpha power for correct and error antisaccade trials (Fig. 2*D*, bottom). The two-way ANOVA showed a significant main effect of depth ($F_{(8,208)} = 38.35$, $p < 1 \times 10^{-20}$), no effect of performance ($F_{(1,28)} = 0.11$, $p = 0.74$), and no interaction effect ($F_{(8,26)} = 1.32$, $p = 0.23$). Likewise, the analysis of gamma power for error and correct antisaccade trials (Fig. 2*D*, top) only showed a significant main effect of depth ($F_{(8,208)} = 10.33$, $p = 3.8 \times 10^{-12}$), but not performance ($F_{(1,26)} = 1.37$, $p = 0.25$) or interaction of depth and performance ($F_{(8,26)} = 0.98$, $p = 0.45$). An ANOVA on gamma power for correct and error antisaccade trials (Fig. 2*D*, bottom) also only revealed an effect of depth ($F_{(8,208)} = 11.91$, $p < 1 \times 10^{-10}$), but not of performance ($F_{(1,26)} = 0.52$, $p = 0.70$) and no interaction effect ($F_{(8,26)} = 1.33$, $p = 0.23$). Together, these findings show depth-dependent alpha and gamma power in area 8Ad and area LIP, but only task-selective and performance-selective alpha and gamma power in area 8Ad.

To test whether preparatory alpha or gamma power could predict task performance on a single trial, we performed linear discriminant analyses (see Materials and Methods). This analysis determined the success rate on which a single trial could be classified into the appropriate response population (correct antisaccade trials or error trials). The classification rates averaged across all 23 sessions were very low for alpha (49.94–51.40%) and gamma power (48.72–51.73%) for the different recording depths, with significant differences only at 450 μm below the cortical surface for gamma power (mean classification rate 51.73%, Wilcoxon signed-rank test against a median of 50, $z = 2.07$, $p = 0.038$). However, in some sessions, single trials could be classified above chance levels. In 30% (7/23) of the sessions, alpha power recorded at a depth of 1050 μm below the cortical surface was predictive of task performance (57.3% mean correct classification rate, range 52.2–70%). This was also the case in 39% (9/23) of the sessions using gamma power at 450 μm below the surface (55.1% mean correct classification rate, range 52.7–60.5%).

Single unit activity during the preparatory period

We next investigated single neuron activity recorded at different depths in area 8Ad and area LIP during the preparatory period (Fig. 3). For these analyses, we grouped neurons into upper layer neurons, recorded at depths between 150 and 900 μm below the cortical surface, and deeper layer neurons, recorded at depths >900 μm (see Materials and Methods).

Neurons in the upper layers of area 8Ad were more active (Wilcoxon signed-rank test, $z = 3.31$, $p = 0.0009$) for prosaccades (7.12 ± 1.15 spikes/s) than antisaccades (6.45 ± 1.16 spikes/s) during the preparatory period. Neurons in upper layers were also significantly more active on error trials (7.73 ± 1.38 spikes/s) than on correct antisaccade trials (6.82 ± 1.38 spikes/s) (Wilcoxon signed-rank test, $z = 2.26$, $p = 0.02$). Neurons in deeper layers did not exhibit different activity between prosaccade (6.87 ± 0.1.12 spikes/s) and antisaccade (6.65 ± 1.15 spikes/s) trials (Wilcoxon signed-rank test, $z = 0.47$, $p = 0.63$) during this prestimulus period. There were also no differences between error and correct trials in deeper layers (7.05 ± 1.11 vs 6.96 ± 2.0 Wilcoxon signed-rank test, $z = 1.31$, $p = 0.19$) during the preparatory period.

In area LIP, there were no differences in discharge rate between prosaccades and antisaccades in the upper layers (6.19 ± 0.87 and 6.14 ± 0.81, Wilcoxon signed-rank test, $z = 0.48$, $p = 0.63$) or deeper layers (7.84 ± 1.07 and 7.32 ± 0.92, Wilcoxon signed-rank test, $z = 1.03$, $p = 0.30$). On error trials, neurons in upper layers were more active (6.24 ± 0.94 spikes/s) than in correct antisaccade trials (5.67 ± 0.8 spikes/s) (Wilcoxon signed-rank test, $z = 2.19$, $p = 0.028$). No differences were found between error and correct trials for neurons in deeper layers (7.35 ± 0.89 versus 7.2 ± 0 0.81 spikes/s, Wilcoxon signed-rank test, $z = 0.36$, $p = 0.71$).

These findings show that neurons in the upper layers of area 8Ad, corresponding to the marmoset FEFs, show task-selective and performance-related preparatory activity that is consistent with proactive inhibitory control.

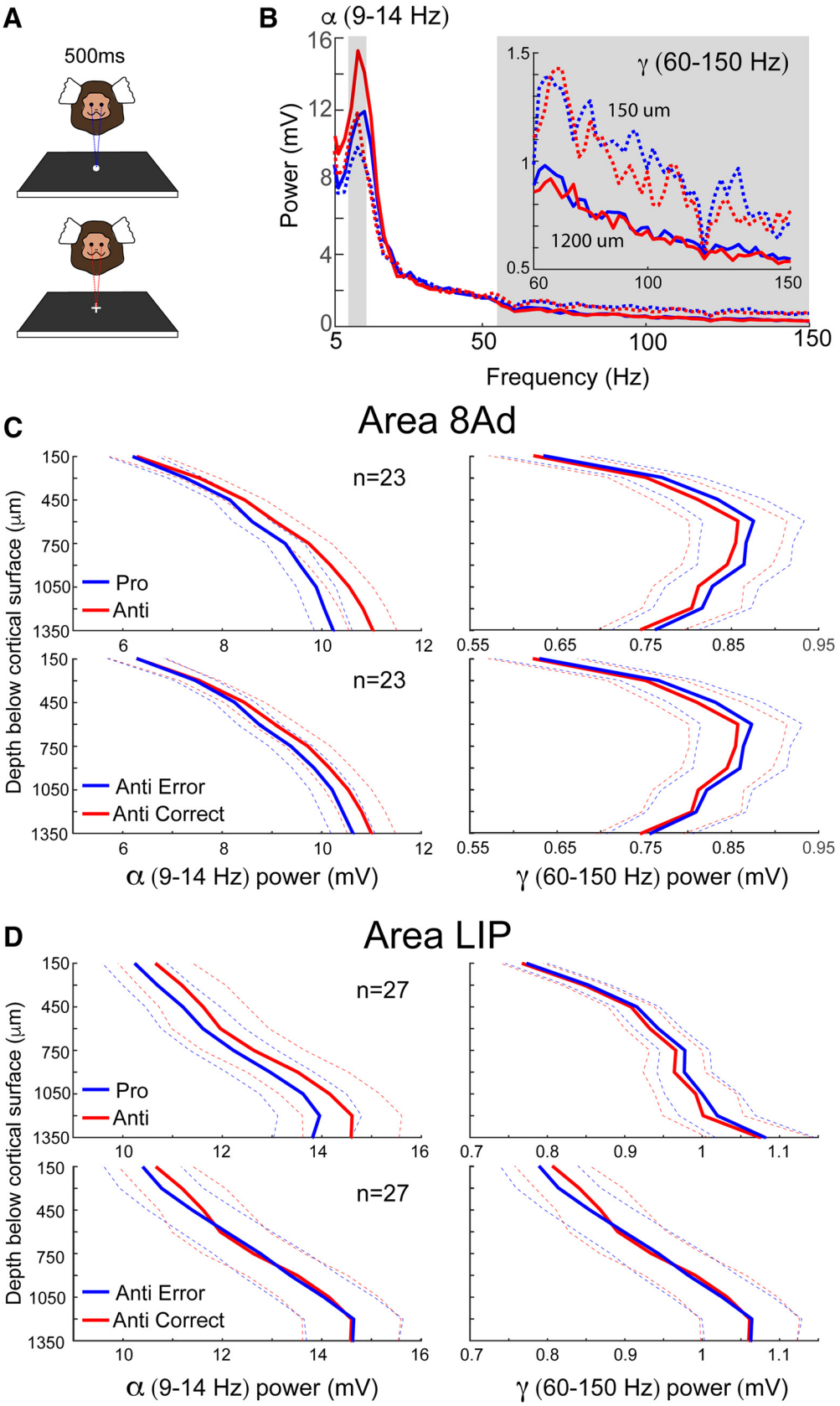

Figure 2. LFP power as a function of frequency band and depth during the preparatory period in areas 8Ad and LIP. ***A***, Preparatory period. Marmosets were maintaining fixation on central instruction cue. Analysis epoch was 500 ms before peripheral stimulus onset. ***B***, LFP power spectrum on prosaccade (blue lines) and antisaccade (red lines) trials for electrode locations 150 (dashed lines) and 1200 μm (sold lines) below the cortical surface. Main depicts LFP power as a function of task and depth in the alpha band (inset) rescaled to highlight differences in the gamma band. ***C***, LFP power in alpha (left), and gamma (right) bands as a function of depth for area 8Ad. Top, Alpha and gamma power as a function of depth on prosaccade (blue lines) and antisaccade (red lines) trials. Bottom, Same as top, but for correct (red lines) and erroneous (blue lines) antisaccade trials. Dashed lines represent SEs. ***D***, same as ***C*** but for area LIP.

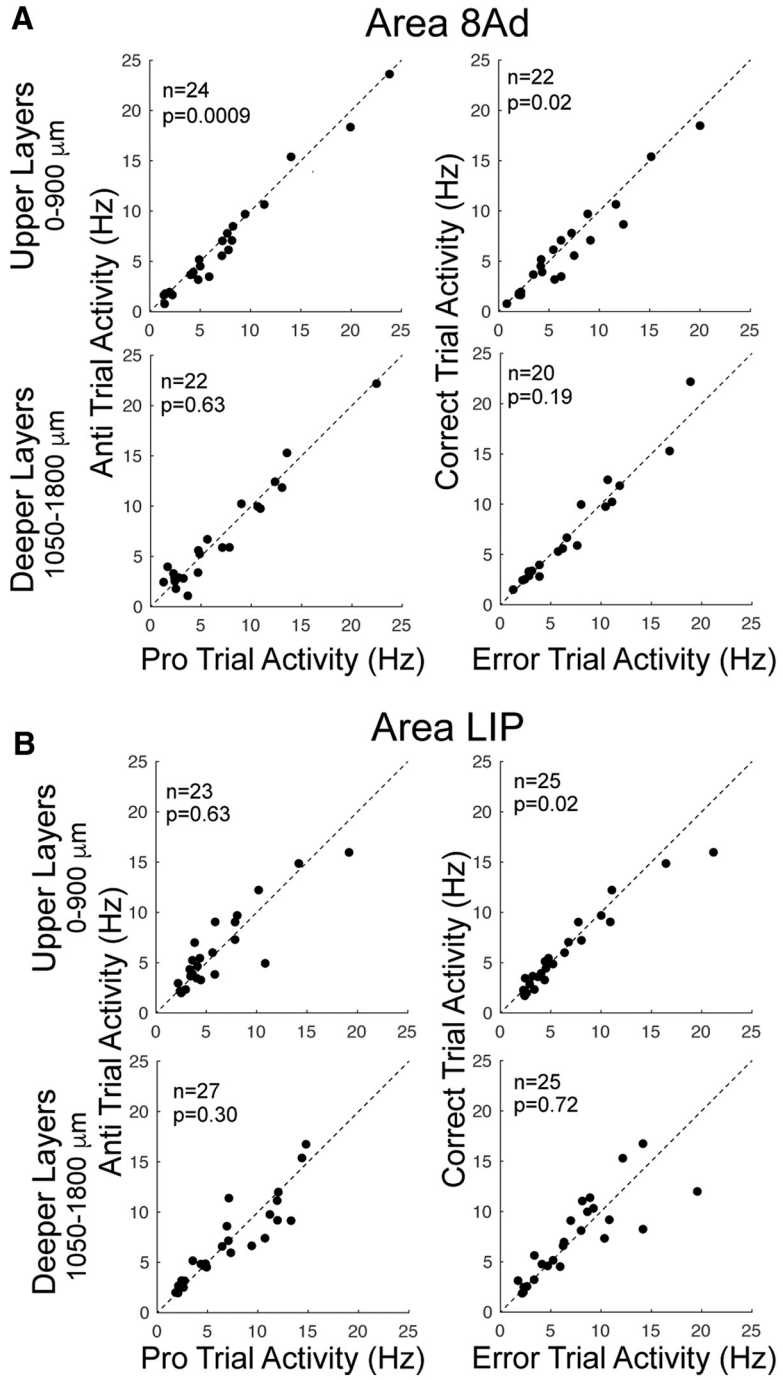

Figure 3. Discharge rate of single neurons in two cortical depth categories on prosaccade and antisaccade trials in areas 8Ad and LIP. ***A***, Area 8 Ad. Left, Scatterplots depicting relative discharge rates on correct prosaccade and antisaccade trials in upper (top) and deeper (bottom) layers. Right, Relative discharge rates on correct and error antisaccade trials in upper (top) and deeper (bottom) layers. ***B***, Same as ***A*** but for parietal area LIP.

troughs. Figure 4 shows neural activity in upper and deeper FEF and LIP aligned on the trough for high and low alpha cycles (Fig. 4, left and right, respectively). These results show that, particularly for high alpha, neural activity was suppressed at the trough of the alpha cycle in the upper area 8Ad layer (Wilcoxon signed-rank test, $z = 4.27$, $p < 2 \times 10^{-5}$) and the upper LIP layer (Wilcoxon signed-rank test, $z = 3.23$, $p = 0.0012$). For upper layer area 8Ad neurons, the modulation index of the discharge rate during the strong alpha trough was higher than during the weak alpha trough (0.095 vs 0.03, Wilcoxon signed-rank test, $z = 2.95$, $p = 0.0032$). No difference between high- and low-alpha troughs was found for deeper FEFs neurons (0.05 vs 0.03, Wilcoxon signed-rank test, $z = 0.02$, $p = 0.98$), upper LIP neurons (0.10 vs 0.08, Wilcoxon signed-rank test, $z = 1.14$, $p = 0.26$), or deeper LIP neurons (0.06 vs 0.04, Wilcoxon signed-rank test, $z = 0.18$, $p = 0.86$).

Cross-frequency coupling between alpha phase and gamma power

To test whether task preparation was associated with cross-frequency interactions between deeper and upper layers in area 8Ad, we quantified how high-frequency activity variations in upper layers related to the phases of slow-frequency activity modulations in deeper layers (Fig. 5). Across all 396 channel pairs, we found a significant cross-frequency increase in correlations between the alpha phase in deeper layers and of ~100–120 Hz gamma-frequency activity in upper layers on antisaccade trials (cluster-based permutation test, $p < 0.001$; Fig. 5*C*). Next, we characterized the alpha phase at which gamma-activity modulations aligned to correct prosaccades and antisaccades and antisaccade error trials for the channel pairs. The polar plot in Figure 5*D* shows the histogram of the preferred phase among all channel pairs. Across LFP pairs, gamma bursts phase locked to the rising phase of the alpha cycle at 300°, with significant nonuniform distributions for all trial types (Rayleigh's z test, prosaccades, $z = 31.5$, $p = 1.2 \times 10^{-14}$; correct antisaccades, $z = 54.3$, $p = 3.6 \times 10^{-25}$; error antisaccades, $z = 45.7$, $p = 3.8 \times 10^{-21}$). The distributions were significantly different between prosaccade and antisaccades (goodness of fit test: $\chi^2 = 36.3$, df = 11, $p = 1.5 \times 10^{-4}$), indicating that alpha phase with gamma activity correlations are task dependent. Additionally, the preferred alpha phase of gamma activities preceding erroneous antisaccades was distinct from both the preferred phase on prosaccade trials ($\chi^2 = 21.9$, df = 11, $p = 0.025$) and that on correct antisaccade trials ($\chi^2 = 37.8$, df = 11, $p = 8.4 \times 10^{-5}$). Because prosaccades were made on erroneous antisaccade trials, we inves-

Influence of alpha power on single unit activity

The previous analyses showed that alpha power was enhanced in deeper layers and single neuron activity was reduced in upper layers on antisaccade trials in FEFs. This suggests that deep alpha may inhibit the discharge of upper FEF neurons. To directly test this hypothesis, we computed average alpha phase-aligned single neuron activity during the preparatory period (see Materials and Methods). To test whether stronger alpha has a larger inhibitory effect than weaker alpha, we performed a median split of the aligned spiking activities based on the magnitude of the alpha

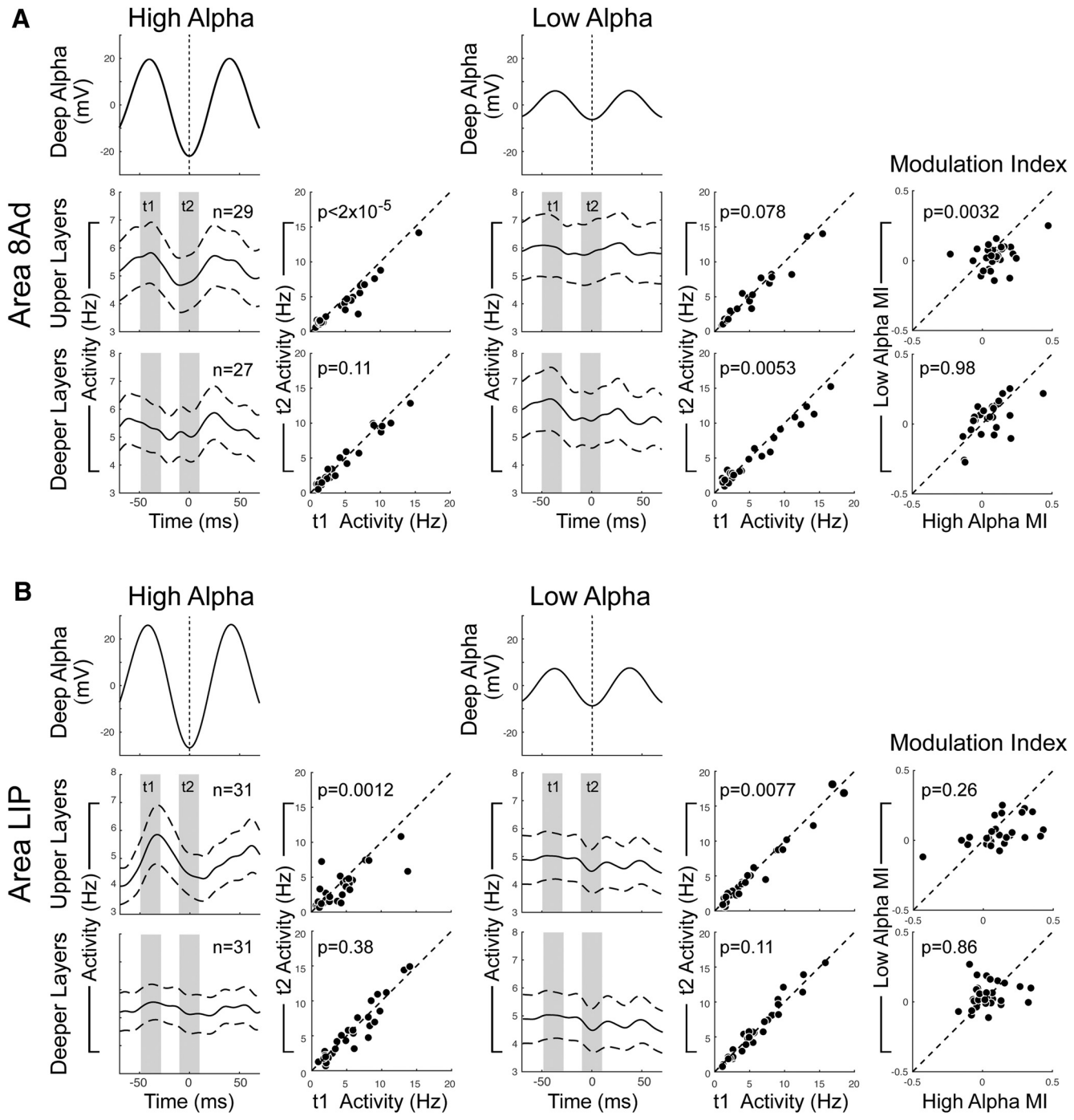

Figure 4. Discharge rates of single neurons in upper and deeper cortical layers in relation to phase and magnitude of the LFP alpha cycle. ***A***, Area 8 Ad. Leftmost five panels, Data from trials with high-amplitude alpha as determined by median split (see Materials and Methods). Top left, Mean LFP recorded at 1350 μm below the cortical surface, filtered between 9 and 14 Hz, and aligned on trough of the alpha cycle. Middle left, Single neuron discharge mean $\pm$ SEM in upper layers as a function of time aligned on trough of the alpha cycle. Shaded windows depict 20 ms epochs aligned on peak (t1) and trough (t2) of alpha cycle, within which mean discharge rates of single neurons were determined. Bottom left, Same as middle but for deeper layers. Scatterplots depict mean discharge rates in epoch t1 plotted against that in epoch t2 for upper (middle) and deeper (bottom) layers, respectively. Five panels to immediate right, same as leftmost panels but for low-amplitude alpha as determined by median split. Panels to extreme right, Top, modulation index of single neuron discharge rates on low alpha trials plotted against that on high alpha trials. Top, Upper layers; bottom, deeper layers. ***B***, Area LIP. Description same as for area 8 Ad above.

tigated whether the distribution of the preferred phases preceding such errors would resemble the distribution preceding correct prosaccades more than it does the distribution from the correct antisaccade trials. To do this, we built a difference distribution of gamma amplitudes by taking the difference between the products of mean amplitudes and their corresponding probability from the error (antisaccade) trials and the correct antisaccade trials before calculating the circular mean and finding the preferred alpha-phase angle for each channel pair. The same was done for the difference between error trials and correct prosaccade trials. We did not find a significant difference between the preferred phase of the two newly constructed distributions (goodness of fit test: $\chi^2 = 6.29$, df $= 11$, $p = 0.85$). Therefore, although prosaccades were made as erroneous responses on an-

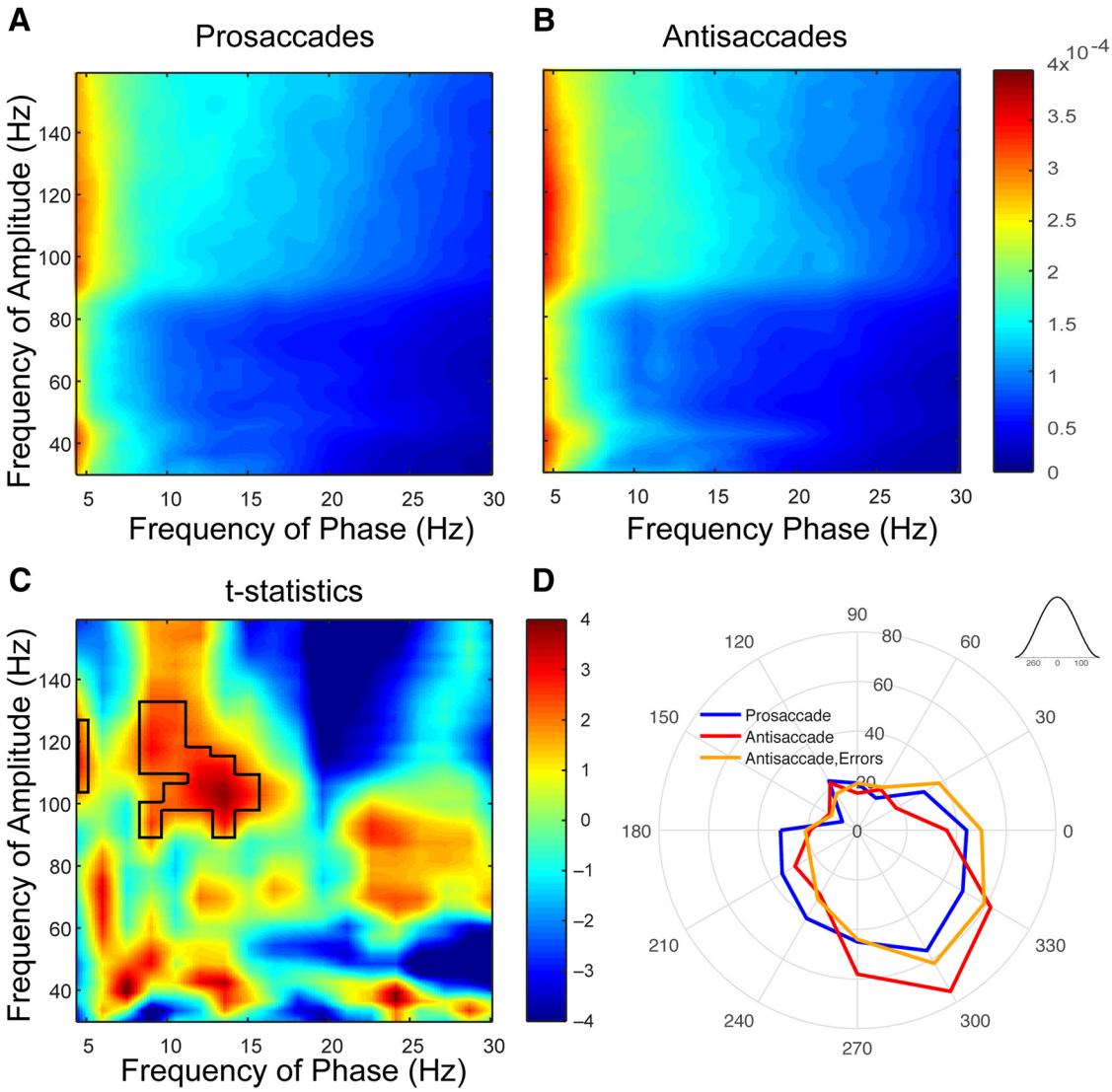

Figure 5. Correlations between deep layer alpha phase and upper layer gamma amplitude on prosaccade and antisaccade trials. ***A***, Comodulogram depicting the normalized MI quantifying the correlation between low-frequency LFP phase in deeper layers with high-frequency amplitude in upper layers on prosaccade trials (see Materials and Methods). ***B***, Same as ***A*** but for antisaccade trials. ***C***, Co-modulogram of *t* statistics between the RSI of real and surrogate data. The RSI quantified rule-related difference in the MI: positive values signify stronger MI during antisaccade trials and negative values signify strong MI during prosaccade trials. Area within black lines depicts significant positive *t* statistics ($p < 0.001$, see Materials and Methods). Significant variations of the RSI reflect correlations between deep layer alpha phase and upper-level gamma amplitude selectively on antisaccade trials. ***D***, Polar plot depicting preferred phase of alpha oscillation for gamma activity on correct prosaccade and antisaccade trials and antisaccade error trials for all channel pairs. Alpha– gamma MIs were highest on the rising phase at 300° of the alpha cycle and their magnitudes were task specific.

tisaccade trials, the neural processes as reflected in preferred phase of gamma activities before these errors did not resemble those before correct prosaccades.

Discussion

Numerous studies have linked alpha oscillations to perceptual processes (Varela et al., 1981; VanRullen and Koch, 2003; Ergenoglu et al., 2004; Thut et al., 2006; Busch et al., 2009; Haegens et al., 2011; Bonnefond and Jensen, 2015; Milton and Pleydell-Pearce, 2016). More recently, alpha power and phase have also been implicated in voluntary saccade control in humans (Hamm et al., 2012a,b; Hwang et al., 2014, 2016). Here, we took advantage of the lissencephalic cortex in marmoset monkeys and recorded laminar neural activity in two main nodes of the frontoparietal saccade network. Consistent with findings from MEG recordings (Hwang et al., 2014, 2016) in humans, we found stronger alpha power in area 8Ad, the putative marmoset FEF (Ghahremani et al., 2017), on antisaccade compared with prosaccade trials and weaker alpha power when monkeys failed to suppress a saccade toward the stimulus. Consistent with recent laminar recordings in other frontal areas in macaques (Bastos et al., 2018), we found also that LFP alpha power was strongest in deeper layers, whereas gamma power was strongest in upper layers of area 8Ad. Our findings support a model in which alpha activity in deeper cortical layers inhibits upper spiking activity for proactive saccade control in the FEF.

Task-related differences in FEFs

Different levels of spiking activity between prosaccade and antisaccade trials have been reported for most cortical and subcortical areas of the saccade network in macaque monkeys, including the FEFs (Everling and Munoz, 2000). In the FEFs, saccade-related neurons are less active for antisaccade than for prosaccade trials during the preparatory period, consistent with proactive

inhibition in these areas on antisaccade trials. Here, we found a similar result for marmoset FEF neurons in the upper layers, whereas the population of deeper FEF neurons failed to show significant task-related differences during the preparatory period. This finding may be surprising given that neurons that were identified as layer V neurons using antidromic stimulation of the SC in macaques were more active for prosaccades than for antisaccades (Everling and Munoz, 2000). We believe that this difference is likely related to differences in neural sampling between the two studies. Although we included here all neurons that could be isolated, only neurons with saccade-related activity were included in the former macaque study. Therefore, whereas our data show that task selectivity is prominent in upper FEF neurons, it is not inconsistent with previous macaque data demonstrating task selectivity in a subset of FEF neurons in deeper layers. Indeed, the presence of higher-gamma power for prosaccades throughout the cortical layers in FEF indicates task selectivity in deeper FEF layers in marmosets.

It should be noted that, although we observed differences in alpha and gamma power between correct and error antisaccade trials, these differences were poor predictors of trial outcome when considered on a trial-by-trial basis. We attribute this to several potential factors. First, previous studies investigating differences in preparatory activity between correct and error antisaccade trials in the FEFs (Everling and Munoz, 2000) and SC (Everling et al., 1998) have shown that significant differences in spiking activity between correct and error trials appears only late in the preparatory period, the period 40–50 ms after stimulus onset but before saccade onset. The late onset and short duration of these differences may be difficult to capture in the power of the periodic LFP signal. Second, we did not attempt to optimize our stimulus presentation with respect to the response fields of the neurons under study because this is impractical with multicontact probes sampling a relatively large cortical area. In the SC, it has been shown the ability of a trial by trial discriminant analysis to predict outcomes on antisaccade trials declines substantially when the visual stimulus is presented outside of the response field (Everling et al., 1998). Because broad spatial tuning of LFP responses has been observed in macaque FEFs (Babapoor-Farrokhran et al., 2017), it seems likely that nonoptimal stimulus presentation at some sites affected our results here. Finally, the more general consideration of trial-by-trial variability in neural responses may have played a role. It has been well established that neural responses between even identical stimulus presentations vary considerably (Tolhurst et al., 1983; Kelly et al., 2010) due to factors such as variation in the intrinsic states of neural networks and random noise fluctuations in neurons (Faisal et al., 2008). Such variability may also have contributed to low classification rates of correct and error antisaccade trials based on single trial LFP power. It should be noted that even the successful mean classification rate for single SC neuron activity in the period 40–50 ms after stimulus onset is only 68% (Everling et al., 1998) compared with the 57% that we found for 30% of the sessions here.

Deep alpha suppresses neural activity in upper layers of area 8Ad

Alpha oscillations are the most prominent feature of the awake human brain (Berger, 1929). Although they have long been interpreted as simply reflecting "cortical idling" (Pfurtscheller et al., 1996), there is now strong evidence that alpha oscillations play an important role in perceptual, motor, and cognitive processes. Detection of a visual stimulus, for example, is reduced on trials with high alpha power (Ergenoglu et al., 2004; Thut et al., 2006) and the phase of ongoing alpha oscillations in the EEG predicts visual detection (Busch et al., 2009; Milton and Pleydell-Pearce, 2016). By recording in the somatosensory cortex in a macaque monkey, Haegens et al. (2011) showed that alpha power decreased during a vibrotactile discrimination task and that lower alpha power was associated with better detection performance. In addition, spiking activity was directly modulated by the phase of the alpha cycle. A similar result was obtained in a human MEG study that showed a decrease in alpha power at the trough of the alpha cycle (Bonnefond and Jensen, 2015). These results are consistent with the pulsed inhibition model (Varela et al., 1981; VanRullen and Koch, 2003), according to which pulses of alpha inhibit spiking and gamma activity every 100 ms. Jensen and colleagues (Jensen and Mazaheri, 2010; Gips et al., 2016) proposed that such a "pulsed inhibition" serves to functionally disengage a region from a network. Accordingly, the stronger alpha power in FEF may also disengage this important saccade-related area from the saccade network on antisaccade trials to reduce the probability of an unwanted automatic saccade toward the upcoming potent stimulus.

In macaques, alpha oscillations are strongest in deep cortical layers in both visual (Maier et al., 2010; Buffalo et al., 2011; van Kerkoerle et al., 2014) and frontal cortical areas (Bastos et al., 2018) and the phase of deep alpha modulates the power of upper gamma (Spaak et al., 2012). Here, we show a similar pattern in marmoset area 8Ad. with strong alpha power in deeper layers. which modulates spiking activity in upper layers in a phase-dependent manner, namely a suppression of activity at the trough of the alpha cycle.

The strong alpha power in deeper area 8Ad layers may directly originate locally within the deep layers where neurons intrinsically burst at alpha frequencies (Silva et al., 1991). These neurons suppress activity throughout the cortical column via polysynaptic inhibition, corresponding to the trough of the alpha cycle (Olsen et al., 2012). In parallel, thalamocortical projections also provide alpha-paced pulsed signals to layers 4, 5, and 6 (Constantinople and Bruno, 2013). Although neurons in the mediodorsal thalamus do not express different activities for prosaccade and antisaccades during the preparatory period, many neurons in the ventroanterior and ventrolateral thalamus are more active for antisaccades during this period (Kunimatsu and Tanaka, 2010), making them possible sources for task-dependent pulsed inhibition to the FEFs.

Absence of task-related differences in parietal cortex

In addition to FEF, some human fMRI studies have reported higher preparatory activation for antisaccades than for prosaccades in the intraparietal sulcus (IPS) (DeSouza et al., 2003; Brown et al., 2007), although another study did not find such signals (Connolly et al., 2002). Here, we did not find any significant differences in alpha power, gamma power, or population single neuron activity between the two tasks in marmoset parietal area LIP during the preparatory period. This is consistent with the earlier described human FEF MEG study that also did not find task-selective alpha power in the IPS (Hwang et al., 2014). Hwang and colleagues (Jensen and Mazaheri, 2010; Gips et al., 2016) speculated that IPS may be more involved in the vector inversion process, which can only start after peripheral stimulus presentation, not in setting the preparatory state for the task.

Marmosets as an additional nonhuman primate model for cognitive saccade control

Recently, marmoset monkeys have garnered a great deal of attention due primarily to their potential as transgenic primate models (Sasaki et al., 2009; Izpisua Belmonte et al., 2015), but also for practical reasons such as their small size, relative ease of handling, breeding potential, and their lissencephalic cortex, which allows access to cortical areas that are buried in sulci in macaques (Mitchell and Leopold, 2015). Although it had been shown that marmosets can be trained to perform simple visually guided eye movement tasks under head restraint (Mitchell et al., 2014; Johnston et al., 2018), it remained unclear whether they could perform more cognitive saccade tasks such as antisaccades. Here, we found that marmosets could be trained to perform up to the final antisaccade training stage for macaques within in a few months. In this final stage of training, a very small and dim stimulus is still present at the mirror location of the peripheral stimulus, cueing the target location for the antisaccades. Although the final step from this cued task to an antisaccade to an unmarked location is also challenging for most macaques, we found that the two marmosets in this study could not consistently perform antisaccades without such a visual cue. We thus stopped the training at this point and began the laminar recordings. Saccades toward the small stimulus have the same properties as antisaccades in macaques (Bell et al., 2000) and humans (Dafoe et al., 2007), including longer reaction times, higher error rates, and shorter response errors. Most importantly, although this task does not require the geometrical calculation of vector inversion, it retains the need for saccade inhibition and for voluntary saccade generation, clinically the most important features of the antisaccade task. Indeed, many studies in humans (Barton et al., 2002; Edelman et al., 2006; Aponte et al., 2018) also cue the peripheral saccade targets to facilitate vector inversion.

Conclusion

Our findings support a model in which alpha power in deep cortical layers provides a pulsed inhibition signal to both deeper and upper cortical layers. Modulation of the strength of these alpha pulses may be the mechanism through which proactive saccade control is instantiated in the primate FEFs. In fact, reduced alpha power has been found in human populations known to exhibit impairments in the antisaccade task such as adolescents and patients with neuropsychiatric conditions such as schizophrenia (Everling and Fischer, 1998; Hutton and Ettinger, 2006). Reduced alpha power has been directly observed in adolescents during the preparatory period on antisaccade trials (Hwang et al., 2016). Likewise, schizophrenia patients have long been known to exhibit reduced alpha power (Moran and Hong, 2011). Therefore, failure to increase alpha power on antisaccade trials during task preparation may be the underlying common neural basis of a saccade suppression deficit.

References

Antoniades C, Ettinger U, Gaymard B, Gilchrist I, Kristjánsson A, Kennard C, John Leigh R, Noorani I, Pouget P, Smyrnis N, Tarnowski A, Zee DS, Carpenter RH (2013) An internationally standardised antisaccade protocol. Vision Res 84:1–5.

Aponte EA, Tschan DG, Stephan KE, Heinzle J (2018) Inhibition failures and late errors in the antisaccade task: Influence of cue delay. J Neurophysiol 120: 3001–3016.

Babapoor-Farrokhran S, Vinck M, Womelsdorf T, Everling S (2017) Theta and beta synchrony coordinate frontal eye fields and anterior cingulate cortex during sensorimotor mapping. Nat Commun 8:13967.

Barton JJ, Cherkasova MV, Lindgren K, Goff DC, Intriligator JM, Manoach DS (2002) Antisaccades and task switching: studies of control processes in saccadic function in normal subjects and schizophrenic patients. Ann N Y Acad Sci 956:250–263.

Bastos AM, Loonis R, Kornblith S, Lundqvist M, Miller EK (2018) Laminar recordings in frontal cortex suggest distinct layers for maintenance and control of working memory. Proc Natl Acad Sci U S A 115:1117–1122.

Bell AH, Everling S, Munoz DP (2000) Influence of stimulus eccentricity and direction on characteristics of prosaccade and antisaccades in nonhuman primates. J Neurophysiol 84:2595–2604.

Berens P (2009) Circstat: A MATLAB toolbox for circular statistics. Journal of Statistical Software. Available at https://doi.org/10.18637/jss.v031.i10

Berger H (1929) Über das elektrenkephalogramm des menschen. Archiv für Psychiatrie und Nervenkrankheiten 87:527–570.

Bonnefond M, Jensen O (2015) Gamma activity coupled to alpha phase as a mechanism for top-down controlled gating. PLoS One 10:e0128667.

Brown MR, Vilis T, Everling S (2007) Frontoparietal activation with preparation for antisaccades. J Neurophysiol 98:1751–1762.

Bruce CJ, Goldberg ME (1985) Primate frontal eye fields. I. Single neurons discharging before saccades. J Neurophysiol 53:603–635.

Bruce CJ, Goldberg ME, Bushnell MC, Stanton GB (1985) Primate frontal eye fields. II. Physiological and anatomical correlates of electrically evoked eye movements. J Neurophysiol 54:714–734.

Buffalo EA, Fries P, Landman R, Buschman TJ, Desimone R (2011) Laminar differences in gamma and alpha coherence in the ventral stream. Proc Natl Acad Sci U S A 108:11262–11267.

Busch NA, Dubois J, VanRullen R (2009) The phase of ongoing EEG oscillations predicts visual perception. J Neurosci 29:7869–7876.

Connolly JD, Goodale MA, Menon RS, Munoz DP (2002) Human fMRI evidence for the neural correlates of preparatory set. Nat Neurosci 5:1345–1352.

Constantinople CM, Bruno RM (2013) Deep cortical layers are activated directly by thalamus. Science 340:1591–1594.

Curtis CE, D'Esposito M (2003) Success and failure suppressing reflexive behavior. J Cogn Neurosci 15:409–418.

Dafoe JM, Armstrong IT, Munoz DP (2007) The influence of stimulus direction and eccentricity on pro- and anti-saccades in humans. Exp Brain Res 179:563–570.

DeSouza JF, Menon RS, Everling S (2003) Preparatory set associated with pro-saccades and anti-saccades in humans investigated with event-related FMRI. J Neurophysiol 89:1016–1023.

Edelman JA, Valenzuela N, Barton JJ (2006) Antisaccade velocity, but not latency, results from a lack of saccade visual guidance. Vision Res 46: 1411–1421.

Ergenoglu T, Demiralp T, Bayraktaroglu Z, Ergen M, Beydagi H, Uresin Y (2004) Alpha rhythm of the EEG modulates visual detection performance in humans. Brain Res Cogn Brain Res 20:376–383.

Everling S, Fischer B (1998) The antisaccade: a review of basic research and clinical studies. Neuropsychologia 36:885–899.

Everling S, Munoz DP (2000) Neuronal correlates for preparatory set associated with pro-saccades and anti-saccades in the primate frontal eye field. J Neurosci 20:387–400.

Everling S, Dorris MC, Munoz DP (1998) Reflex suppression in the antisaccade task is dependent on prestimulus neural processes. J Neurophysiol 80:1584–1589.

Everling S, Dorris MC, Klein RM, Munoz DP (1999) Role of primate superior colliculus in preparation and execution of anti-saccades and pro-saccades. J Neurosci 19:2740–2754.

Faisal AA, Selen LP, Wolpert DM (2008) Noise in the nervous system. Nat Rev Neurosci 9:292–303.

Ghahremani M, Hutchison RM, Menon RS, Everling S (2017) Frontoparietal functional connectivity in the common marmoset. Cereb Cortex 27: 3890–3905.

Gips B, van der Eerden JP, Jensen O (2016) A biologically plausible mechanism for neuronal coding organized by the phase of alpha oscillations. Eur J Neurosci 44:2147–2161.

Haegens S, Nácher V, Luna R, Romo R, Jensen O (2011) alpha-oscillations in the monkey sensorimotor network influence discrimination performance by rhythmical inhibition of neuronal spiking. Proc Natl Acad Sci U S A 108:19377–19382.

Hamm JP, Sabatinelli D, Clementz BA (2012a) Alpha oscillations and the control of voluntary saccadic behavior. Exp Brain Res 221:123–128.

Hamm JP, Dyckman KA, McDowell JE, Clementz BA (2012b) Pre-cue

fronto-occipital alpha phase and distributed cortical oscillations predict failures of cognitive control. J Neurosci 32:7034–7041.
Hutton SB, Ettinger U (2006) The antisaccade task as a research tool in psychopathology: a critical review. Psychophysiology 43:302–313.
Hwang K, Ghuman AS, Manoach DS, Jones SR, Luna B (2014) Cortical neurodynamics of inhibitory control. J Neurosci 34:9551–9561.
Hwang K, Ghuman AS, Manoach DS, Jones SR, Luna B (2016) Frontal preparatory neural oscillations associated with cognitive control: a developmental study comparing young adults and adolescents. Neuroimage 136:139–148.
Izpisua Belmonte JC, et al. (2015) Brains, genes, and primates. Neuron 86:617–631.
Jensen O, Mazaheri A (2010) Shaping functional architecture by oscillatory alpha activity: gating by inhibition. Front Hum Neurosci 4:186.
Johnston K, Everling S (2011) An approach to understanding the neural circuitry of saccade control in the cerebral cortex using antidromic identification in the awake behaving macaque monkey model. In: Animal models of movement disorders (Lane EL, Dunnett SB, eds). New York: Springer.
Johnston KD, Barker K, Schaeffer L, Schaeffer D, Everling S (2018) Methods for chair restraint and training of the common marmoset on oculomotor tasks. J Neurophysiol 119:1636–1646.
Kelly RC, Smith MA, Kass RE, Lee TS (2010) Local field potentials indicate network state and account for neuronal response variability. J Comput Neurosci 29:567–579.
Kunimatsu J, Tanaka M (2010) Roles of the primate motor thalamus in the generation of antisaccades. J Neurosci 30:5108–5117.
Maier A, Adams GK, Aura C, Leopold DA (2010) Distinct superficial and deep laminar domains of activity in the visual cortex during rest and stimulation. Front Syst Neurosci 4:31.
Maris E, Oostenveld R (2007) Nonparametric statistical testing of EEG- and MEG-data. J Neurosci Methods 164:177–190.
Miller EK, Cohen JD (2001) An integrative theory of prefrontal cortex function. Annu Rev Neurosci 24:167–202.
Milton A, Pleydell-Pearce CW (2016) The phase of pre-stimulus alpha oscillations influences the visual perception of stimulus timing. Neuroimage 133:53–61.
Mitchell JF, Leopold DA (2015) The marmoset monkey as a model for visual neuroscience. Neurosci Res 93:20–46.
Mitchell JF, Reynolds JH, Miller CT (2014) Active vision in marmosets: a model system for visual neuroscience. J Neurosci 34:1183–1194.
Moran LV, Hong LE (2011) High vs low frequency neural oscillations in schizophrenia. Schizophr Bull 37:659–663.
Munoz DP, Everling S (2004) Look away: the anti-saccade task and the voluntary control of eye movement. Nat Rev Neurosci 5:218–228.
O'Driscoll GA, Alpert NM, Matthysse SW, Levy DL, Rauch SL, Holzman PS (1995) Functional neuroanatomy of antisaccade eye movements investigated with positron emission tomography. Proc Natl Acad Sci U S A 92:925–929.
Olsen SR, Bortone DS, Adesnik H, Scanziani M (2012) Gain control by layer six in cortical circuits of vision. Nature 483:47–52.
Paxinos G, Watson C, Petrides M, Rosa MG, Tokuno H (2012) The marmoset brain in stereotaxic coordinates. Oxford: Elsevier.
Pfurtscheller G, Stancák A Jr, Neuper C (1996) Event-related synchronization (ERS) in the alpha band–an electrophysiological correlate of cortical idling: a review. Int J Psychophysiol 24:39–46.
Sasaki E, et al. (2009) Generation of transgenic non-human primates with germline transmission. Nature 459:523–527.
Silva LR, Amitai Y, Connors BW (1991) Intrinsic oscillations of neocortex generated by layer 5 pyramidal neurons. Science 251:432–435.
Spaak E, Bonnefond M, Maier A, Leopold DA, Jensen O (2012) Layer-specific entrainment of gamma-band neural activity by the alpha rhythm in monkey visual cortex. Curr Biol 22:2313–2318.
Thut G, Nietzel A, Brandt SA, Pascual-Leone A (2006) Alpha-band electroencephalographic activity over occipital cortex indexes visuospatial attention bias and predicts visual target detection. J Neurosci 26:9494–9502.
Tolhurst DJ, Movshon JA, Dean AF (1983) The statistical reliability of signals in single neurons in cat and monkey visual cortex. Vision Res 23:775–785.
Tort AB, Komorowski R, Eichenbaum H, Kopell N (2010) Measuring phase-amplitude coupling between neuronal oscillations of different frequencies. J Neurophysiol 104:1195–1210.
van Kerkoerle T, Self MW, Dagnino B, Gariel-Mathis MA, Poort J, van der Togt C, Roelfsema PR (2014) Alpha and gamma oscillations characterize feedback and feedforward processing in monkey visual cortex. Proc Natl Acad Sci U S A 111:14332–14341.
VanRullen R, Koch C (2003) Is perception discrete or continuous? Trends Cogn Sci 7:207–213.
Varela FJ, Toro A, John ER, Schwartz EL (1981) Perceptual framing and cortical alpha rhythm. Neuropsychologia 19:675–686.
Voloh B, Valiante TA, Everling S, Womelsdorf T (2015) Theta-gamma coordination between anterior cingulate and prefrontal cortex indexes correct attention shifts. Proc Natl Acad Sci U S A 112:8457–8462.